A Study of Large-eddy Simulation using Statistical and Machine Learning Techniques

Mohammed Khalid Hossen[*]

Department of Computer Science and Engineering, Sylhet Agricultural University, Sylhet, Bangladesh

ABSTRACT

The numerical solution of Navier-Stokes (N-S) equations has been found useful in various disciplines during its development, especially in recent years. However, a large-eddy simulation method has been developed to model the subgrid-scale dissipation rate by closing the Navier-Stokes equations. Because the instantaneous and time-averaged statistic characteristics of the subgrid-scale turbulent kinetic energy and dissipation have been studied by large eddy simulation. The purpose of this study is to check the statistical and machine learning of the subgrid-scale energy dissipation. As we know that the current turbulence theory states that the vortex stretching mechanism transports energy from large to small scales and leads to a high energy dissipation rate in a turbulent flow. Hence, a vortex-stretching-based subgrid-scale model is considered regarding the square of the velocity gradient to detect the playing role of the vortex stretching mechanism. The study in this article has shown a two-step process. Considering a posteriori statistic of the velocity gradient is analyzed through higher-order statistics and joint probability density function. Secondly, a machine learning approach is studied on the same data. The results of the vortex-stretching-based subgrid-scale model are then compared with the other two dynamic subgrid models, such as the localized dynamic kinetic energy equation model and the TKE-based Deardorff model. The results suggest that the vortex-stretching-based model can detect the significant subgrid-scale dissipation of small-scale motions and predict satisfactory turbulence statistics of the velocity gradient tensor.

Keywords: Navier-Stokes Equations, SGS Models, Vortex Stretching, Subgrid-scale Energy, Subgrid-scale Dissipation, Statistical and Machine Learning, Correlation, JPDF, Gradient Decent Algorithm.

1 Introduction

Over the last few years, the large eddy simulation (LES) technique has increased in popularity, mainly because of advancements in computational resources both in hardware and algorithm. More specifically, recent algorithmic progress in iterative methods, such as multigrid and Krylov solvers on the multiprocessor computing framework, have enabled the LES study of complex engineering flow problems. The main idea of LES is to solve the Navier-Stokes equations (NSE) using a computationally affordable three-dimensional fine grid. It is generally expected that the numerical solution of NSE would account for about 80% of the dominant degrees of freedom of turbulence. The remaining 20% of the information on turbulence is predicted based on the available data from a previous time step through a process called subgrid-scale (SGS) modeling. Smagorinsky initially introduced this idea for real-time weather prediction [1]. Over the years, LES has paved the way to solve many complex engineering problems. More recently, several investigators are advancing LES so that a subgrid model can be built upon available data history.

Another interesting idea of the fluid dynamics research community is to understand whether LES can provide appropriate relevant data that may be used to develop simplified models for studying various complex engineering problems. Turbulence is a high-dimensional dynamical system. It exhibits an average cascade of energy from large to small scales. The resolution large-eddy simulation (LES) approach utilizes subgrid models to understand turbulence energy cascade, which is saving millions of dollars for the automobile and aviation industry. Until recently, following the pioneering work of Taylor [1], there has been a scope on the dominant modern view of whether vortex stretching drives the energy from the largest to the smallest scales

of motion. No one has been reached explicitly on how to engage vortex stretching in subgrid models of LES properly. In contrast, Sagaut & Cambon argue that vortex stretching opposes energy dissipation [3],[4]. They considered the Karman-Harwoth equation [5] and the interpretation that the energy flux from large to small scale would balance the viscous dissipation. Indeed, these findings lead to creating an option for more studies on how vortex stretching reduces dissipation while at the same time acting for the down-scale cascade of energy (e.g., see [4],[8]).

The objective of the present investigation is twofold. First, a parallelized LES code is developed that engages vortex stretching in a subgrid model [6]. To estimate whether vortex stretching drives the energy cascade, we consider high-resolution LES data and compare higher-order statistics of isotropic turbulence, and the velocity gradient tensor is used to investigate many universal characteristics by using joint probability density function (JPDF) regarding three subgrid-scale models. In the second part, the performance of SGS models has been studied through statistical and machine learning approaches.

This article is rearranged sequentially. In section 2, the simulation methodology has been discussed. Initial turbulent flow is discussed in section 3. Validation strategies are shown in section 4. Results of SGS models are shown in section 5. In the result section, models are compared regarding their performance. Finally, a conclusion and future scope have been drawn in section 6.

2 Simulation Methodology

In this article, instead of using explicit filtering operation, the second order finite volume discretization of the flow equation is considered the numerical mesh as an implicit filter. In this filter, the turbulent scales smaller than the grid mesh are known

as unresolved scales, while greater than grid size is called the resolved scales. It is like the operation of a box filter when the filter width is equal to the grid spacing [5],[7].

Now, the filtered equations of continuity and Navier-Stokes equation for incompressible flow can be written as:

$$\frac{\partial \overline{u_\iota}}{\partial x_i} = 0 \qquad (1)$$

$$\frac{\partial \overline{u_\iota}}{\partial t} + \overline{u}_j \frac{\partial \overline{u_\iota}}{\partial x_j} = -\frac{1}{\rho}\frac{\partial \overline{P}}{\partial x_i} + \vartheta \frac{\partial^2 \overline{u_\iota}}{\partial x_i^2} - \frac{\partial \tau_{ij}}{\partial x_j} \qquad (2)$$

Here, τ_{ij} is the subgrid-scale stresses, where $\tau_{ij} = \overline{u_\iota u_J} - \overline{u}_\iota \overline{u}_j$. Most of the subgrid-scale models are based on the eddy-viscosity model because of the Boussinesq hypothesis. The models can compute the deviatoric part of the SGS stress as,

$$\tau_{ij} - \frac{1}{3}\tau_{kk}\delta_{ij} = -2\vartheta_\tau S_{ij} \qquad (3)$$

Eq. (3) is related to SGS stresses to the large-scale strain rate tensor S_{ij}, which is defined by $S_{ij} = \frac{1}{2}\left(\frac{\partial \overline{u_\iota}}{\partial x_j} + \frac{\partial \overline{u_J}}{\partial x_i}\right)$ of the resolved turbulence, δ_{ij} is the Kronecker delta, and ϑ_τ is a subgrid-scale viscosity.

The SGS models in this article are the Wall-Adapting viscosity model (SGS-A), localized dynamic kinetic energy equation model (SGS-B), and kinetic energy-based Deardorff model (SGS-C). A brief mathematical detail of three dynamic SGS models is described below.

2.1 Wall-Adapting Viscosity Model (SGS-A)

The eddy viscosity is evaluated in this subgrid-scale model by using the square of the velocity gradient tensor [6]. The turbulent kinetic energy of SGS-A model is estimated by,

$$k_{sgs} = (\Delta_{les})^2 \frac{\left(S_{ij}^d S_{ij}^d\right)^{3/2}}{\left(S_{ij}S_{ij}\right)^{5/2} + \left(S_{ij}^d S_{ij}^d\right)^{5/4}}$$

Where, Δ_{les} is the computational grid size. Now, the eddy viscosity of SGS-A model is defined as,

$$\vartheta_\tau = C_w \Delta_{les}\sqrt{k_{sgs}} \qquad (4)$$

The term S_{ij}^d is a deviatoric symmetric part of the square of the velocity gradient tensor, known as $S_{ij}^d = \frac{1}{2}\left(G_{ij} + G_{ij}\right) - \frac{1}{3}\delta_{ij}G_{ii}$. Here, G_{ij} is the velocity gradient tensor. However, the term $S_{ij}^d S_{ij}^d$ is related to vortex stretching and the second invariant of the velocity gradient tensor. The term $S_{ij}^d S_{ij}^d = \frac{1}{2}|S\omega| - \frac{1}{3}Q_G^2$ can detect turbulent structures by the rotation rate, strain rate, and vortex stretching rate, which indicates that it adjusts the value of ϑ_τ dynamically on the strength of the vortex stretching rate [8]. Here, $S\omega$ and Q_G are denoted by vortex stretching and second invariant of the velocity gradient tensor. So, this SGS model is a vortex-stretching-based model, where $C_w = 0.325$ for this study.

2.2 Dynamic k-equation Model (SGS-B)

The localized dynamic kinetic energy model was proposed by Kim et. al., which is a kind of similar concept to the dynamic Smagorinsky model [9]. In this model, the eddy viscosity is calculated as $\vartheta_\tau = C_k k_{sgs}^{1/2}\Delta_{les}$. Here C_k is an adjustable model constant, which is calculated dynamically in this subgrid-scale model. In this SGS model, the model coefficients are computed by setting an additional test filter $\tilde{\Delta} = 2\Delta_{les}$ [10]. It is worth

mentioning that the local variation of subgrid-scale energy dissipation can be accounted for in the localized dynamic kinetic energy equation via the dynamic variation of C_k, which is important in many engineering applications.

2.3 k-equation Model (SGS-C)

In the turbulent kinetic energy (TKE) model, the turbulent kinetic energy is obtained by solving the following transport equation [11].

$$\frac{\partial k_{sgs}}{\partial t} + \overline{u}_j \frac{\partial k_{sgs}}{\partial x_j} = -\tau_{ij}S_{ij} - C_e \frac{k_{sgs}^{\frac{3}{2}}}{\Delta_{les}} + \frac{\partial}{\partial x_j}\left(\vartheta_\tau \frac{\partial k_{sgs}}{\partial x_j}\right) \qquad (5)$$

Here, k_{sgs} is the turbulent kinetic energy. The eddy viscosity ϑ_τ is estimated by using k_{sgs} value from Eq. (5) as $\vartheta_\tau = C_k k_{sgs}^{1/2}\Delta_{les}$. Here, the model constant $C_k = 0.094$ and the dissipation constant $C_e = 1.048$ are fixed. This subgrid-scale model is important for LES of atmospheric turbulence.

3 Turbulent Flow Setup

The initialization of the turbulent flow field is based on the kinematic simulation of isotropic turbulence, which is incompressible and consistent with second-order statistics. The given velocity field is generated in the Fourier space based on the following energy spectrum,

$$E(k) = E_a \frac{k^4}{k_0^4}\left(1 + \frac{k^2}{k_0^2}\right)^{\frac{-17}{6}} exp^{-2\frac{k^2}{k_n^2}} \qquad (6)$$

Here, E_a is amplitude and k is the wave number. k_0 and k_n are two wave numbers that control the distribution of $E(k)$. Therefore, we have the kinetic energy $E = \frac{1}{2}\int_\Omega u^2 dx = \int_0^\infty E(k)dk$. Thus, we can choose the values of E_a, k_0 and k_n to ensure a distribution of E. The initial wave number is taken $k_0 = 5$ in Eq. (6) in such a way that the initial velocity would be $u_0 = 10$ m/s, and the Reynolds number $R_e = 5 \times 10^5$ in physical space. In the present LES simulations, the N-S equations are solved in a cubic periodic domain $[0, 2\pi]^3$, which is partitioned into $N_x \times N_y \times N_z = N$, here $N_x = N_y = N_z = 128$ nodes in each direction. The mesh size is $\Delta_{les} = \frac{2\pi}{N}$.

To analyze the relationship between the resolved strain $S_{ij} = \frac{1}{2}\left(\frac{\partial \overline{u_\iota}}{\partial x_j} + \frac{\partial \overline{u_J}}{\partial x_i}\right)$ and the subfilter scale stress $\tau_{ij} = \overline{u_\iota u_J} - \overline{u}_\iota \overline{u}_j$, this article has implemented three subgrid models, such as SGS-A, SGS-B, and SGS-C within an in-house LES code, which is written in C++ and parallelized via the message passing interface (MPI) library through OpenFOAM.

4 Validation Strategies

In this research, the vortex-stretching-based subgrid model SGS-A is validated with the other two subgrid models, say SGS-B and SGS-C. The validation processes are done by the below strategies,
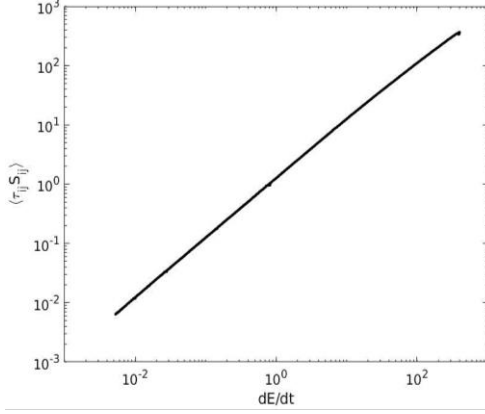
The subgrid-scale production of turbulence $-\tau_{ij}S_{ij}$ must be correlated with the transfer $\tau_{ij}S_{ij}$ from grid-scale to subgrid-scale. It suggests that the transfer of energy is equal to the dissipation (loss) of energy on a subgrid scale.

Joint probability density function (JPDF) and corresponding statistics of the velocity gradient tensor.
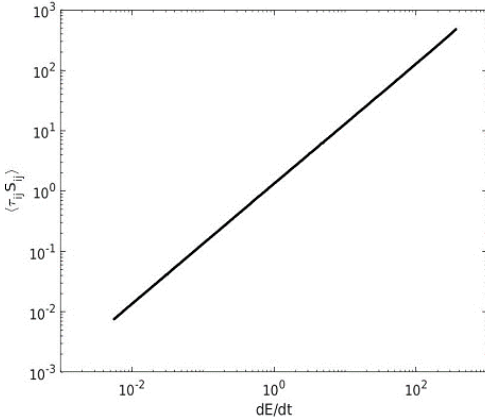
Examine the performance of the three subgrid-scale models through a machine learning algorithm.
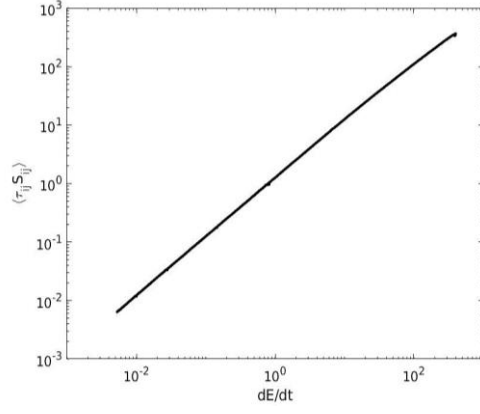
(a) SGS-A

(b) SGS-B

(c) SGS-C

Fig. 1 Plots of production and dissipation of turbulence among the SGS models

5 Result Analyses

5.1 Subgrid-Scale Stress, Resolved Rate of Strain, and Vortex Stretching

Time series of the rate of resolved energy $\frac{dE}{dt}$ is found to be well correlated with the energy flux $< \tau_{ij} S_{ij} >$; Fig. 1 supports the theoretical interpretation regarding the energy flux and viscous dissipation [8]. Indeed, the energy is transferred by large eddies to the subgrid-scale, which is dissipated at a rate of subgrid-scale dissipation, $\varepsilon_{sgs} = 2\vartheta_\tau ||S||$. It is worth mentioning that the most important requirement of turbulence modeling on the statistics of subfilter scale stress τ_{ij} is to reproduce the evolution of turbulence kinetic energy [12]. Thus, the consideration of vortex stretching should correctly reproduce the correlation of a subgrid model τ_{ij}^{sgs} with the strain-rate tensor, i.e., $< \tau_{ij}^{sgs} S_{ij} > = < \tau_{ij} S_{ij} >$. A primary observation is that the consideration of the square of the velocity gradient tensor is an effective way of enforcing scale-adaptivity in ϑ_τ via vortex stretching mechanism. If a vortex tube is stretched, the eddy viscosity grows locally, thereby transferring the energy to the subgrid scale.

5.2 Joint Probability Density Function (JPDF) of SGS Models

In this section, invariants of velocity gradient tensor of isotropic turbulence in LES are analyzed statistically by the proposed three subgrid-scale models. An advanced data-analytics approach is considered to observe some hidden flow topology in subgrid models. Using this approach, five invariants are analyzed to describe the mechanism and dynamics of turbulent flow. Because the invariants are significantly important in the context of visualization of the various flow patterns or coherent structures [13] and detecting the vortical structure of turbulent flow [14]. The datasets of invariants are generated at s fixed dimensionless eddy turn over time, $\frac{t}{T} = 1$. Using the datasets, JPDF of such invariants have been visualized to illustrate the features of small-scale statistics and relevant mechanisms of large energy-containing scales.

The invariants can define the arbitrary points of flow topology by deploying the eigenvalues of the velocity gradient tensor G [15],[16]. Hence, the characteristics equation of the velocity gradient tensor is,

$$\lambda_i^3 + P_G \lambda_i^2 + Q_G \lambda_i + R_G = 0 \qquad (7)$$

Here, λ_i is eigenvalues. P_G, Q_G, and R_G are the first, second, and third invariants of G, respectively. However, for incompressible flow, $P_G = 0$.

The JPDF describes the jointly random variables on a probability space. In this article, The JPDF is studied through: (i) between the second invariant (Q_G) and third invariant (R_G), (ii) between the strain rate of the second invariant (Q_S) and the strain rate of the third invariant (R_S), and (iii) between second invariant rate (-Q_S) and rotation rate (R_S).

Now, Mathematical formulas of such invariants are shown here. Using the strain rate (S_{ij}) and rotation rate (R_{ij}), the second and third invariants of G are obtained by,

$$Q_G = \frac{-1}{2}\left(S_{ij}S_{ij} - R_{ij}R_{ij}\right) \qquad (8)$$

$$R_G = \frac{-1}{3}\left(S_{ij}S_{jk}S_{ki} + \frac{3}{4}\omega_i\omega_j S_{ij}\right) \qquad (9)$$
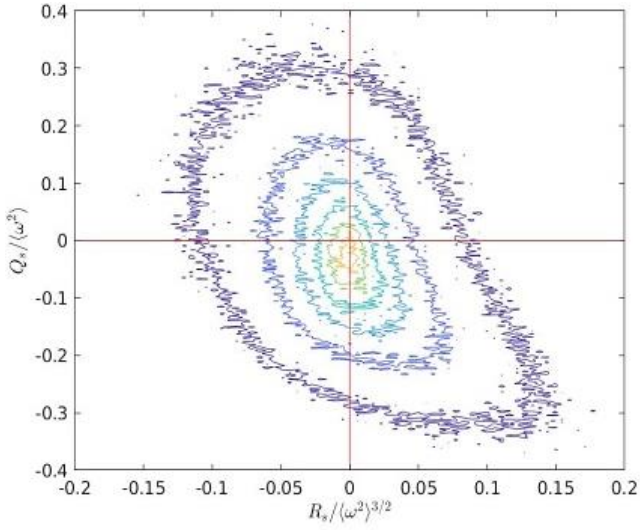
The strain rate of the tensor of second and third invariants are obtained by,
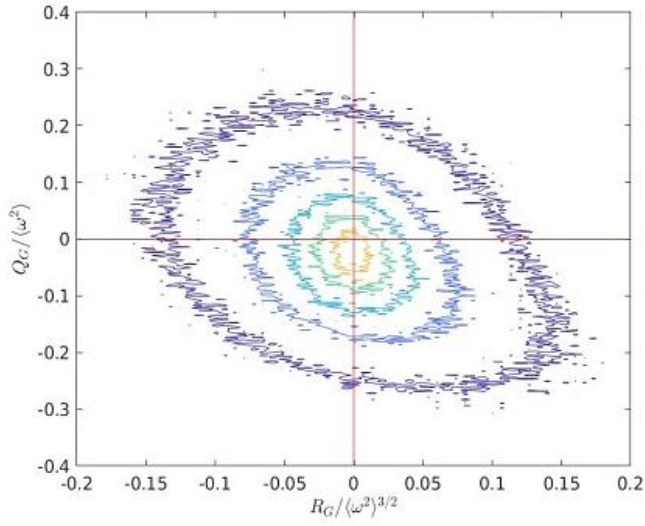
$$Q_S = \frac{-1}{2}\left(S_{ij}S_{ij}\right) \qquad (10)$$

$$R_G = \frac{-1}{3}\left(S_{ij}S_{jk}S_{ki}\right) \qquad (11)$$

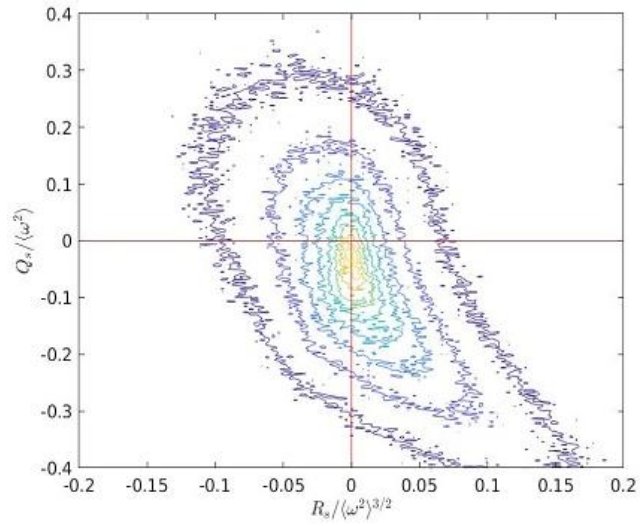Finally, the second invariant rotation rate is getting by,
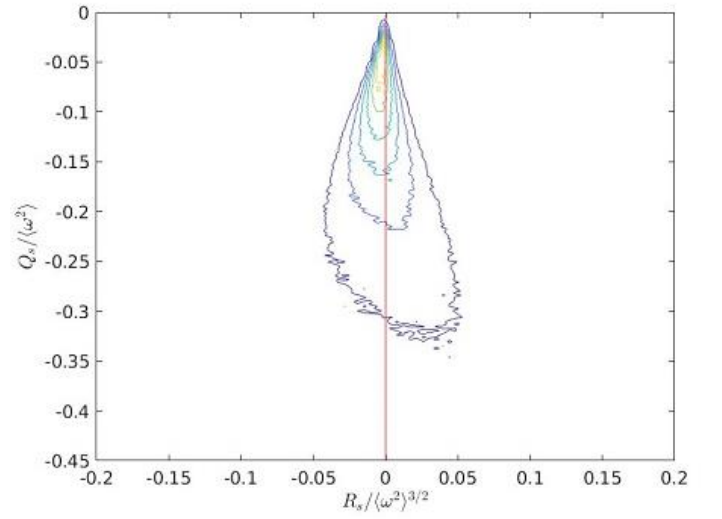
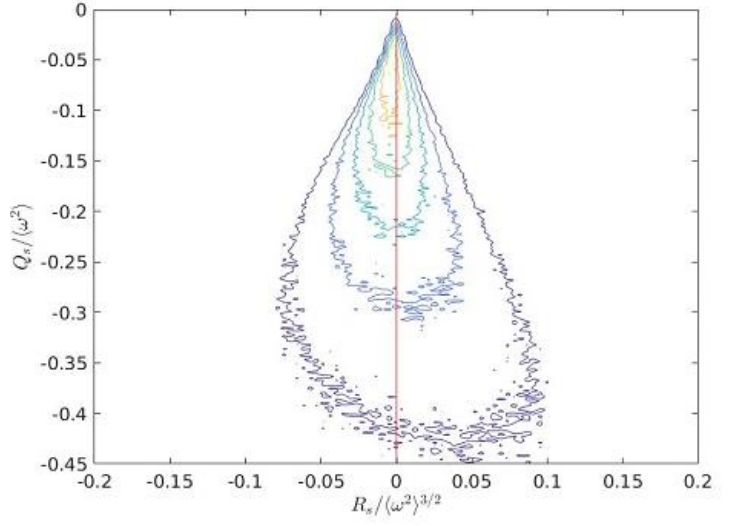$$Q_R = \frac{1}{2}\left(R_{ij}R_{ij}\right) \qquad (12)$$
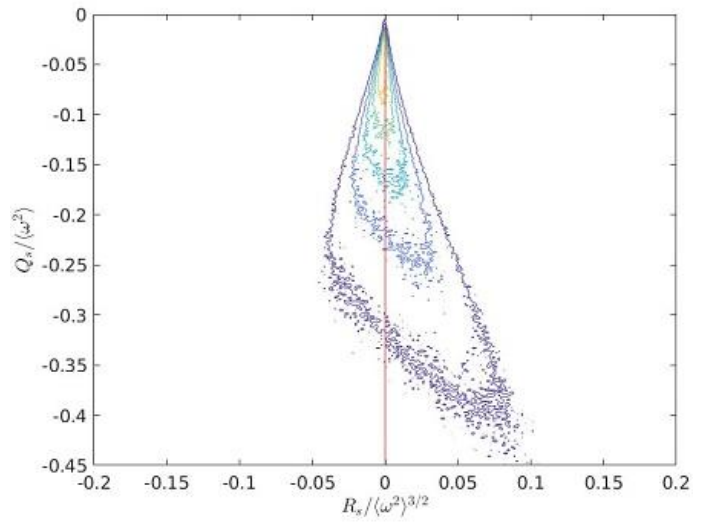
(a)   SGS-A

(a)   SGS-A

(b)   SGS-B

(b)   SGS-B

(c)   SGS-C

(c)   SGS-C

Fig. 2 The JPDF between the second invariant (Q_G) and third invariant (R_G)

Fig. 3 The JPDF between the second invariant of strain rate (Q_S) and third invariant of strain rate (R_S)

The JPDF map between the second invariant (Q_G) and third invariant (R_G), and topological classification of local flow fields are shown in Fig. 2, see more detailed information [8],[15],[16]. The region of Fig. 2 describe as, (i) the region $R_G < 0$ and $Q_G > 0$ is associated with vortex stretching, (ii) the region $R_G > 0$ and $Q_G > 0$ is associated with vortex compression, (iii) the region $R_G < 0$ and $Q_G < 0$ is associated with tube structures, and (iv) the region $R_G > 0$ and $Q_G > 0$ is associated with sheetlike structures. In Fig. 2, two important characteristic features have been observed in the SGS models.

First, a trend of teardrop shape appears in SGS models. In this region, the fluid flow is controlled by the sheetlike structures, which indicates that the total strain rate $S_{ij}S_{ij}$ is increased over weak vortex stretching. It also indicates a universal feature of turbulence [7],[8]. Secondly, the bulk of data is presented in the upper left quadrant showing intense vortex stretching, $\omega_i\omega_j S_{ij} > 0$ in the subgrid-scale models. Hence, the Q_G and R_G map of SGS models indicates that the $\omega_i\omega_j S_{ij}$ and $S_{ij}S_{ij}$ are playing a role for the energy cascade.

The JPDF map between the second invariant of strain rate (Q_S) and third invariant of strain rate (R_S), and topological classification of local flow fields are shown in Fig. 3, see more detailed information [8],[18]. In order to analyze the geometry of the straining motion of the fluid elements, the JPDF of the second invariant of strain rate (Q_S) and third invariant of strain rate (R_S) of the velocity gradient tensor is studied, see Eqs. (10) and (11). All the three SGS models have shown similar behaviour in which the flow topology for isotropic turbulent flow field is predominated by sheetlike structures. Finally, the region $R_S > 0$ and $Q_S < 0$ indicates the intense kinetic energy dissipation in subgrid models, see Fig. 3.

The JPDF map between the second invariant of strain rate ($-Q_S$) and second invariant of rotation rate (Q_w) is shown in Fig. 4. It is an important investigation to demonstrate the dissipation of kinetic energy through rotation rate and straining rate of G. In Fig. 4, the vertical axis $-Q_S$ is associated to the dissipation of kinetic energy [17],[18]. Thus, the points near the axis $-Q_S$ is dominated by the straining motion over weak enstrophy. However, the horizontal axis Q_w is linked to high enstrophy over few dissipations. The most interesting physical information is presented by the diagonal axis, $-Q_S = Q_w$, where it demonstrates the points of flow field associated with the high enstrophy and high dissipation [8]. As we can see in Fig. 4, a strong correlation between dissipation and enstrophy along the diagonal line is presented in SGS models.

5.3 Performance between Subgrid-Scale Models

The correlation is a statistical summary of the relationship between the variables, see for information [19]. This section will focus how on studying the correlation between subgrid-scale model variables. The velocity component U_x of a cell value at $\frac{t}{T} = 1$ eddy turn-over time of the SGS models is considered for this purpose. Approximately 700 samples of U_x are studied in this article see Fig. 5. Specifically, this study will examine how much the velocity component U_x of SGS-A model is associated with U_x of SGS-B and SGS-C models. If we compare the U_x of SGS-A model with the SGS-B and SGS-C models, we get almost similar performance among the subgrid models, see Fig. 6.
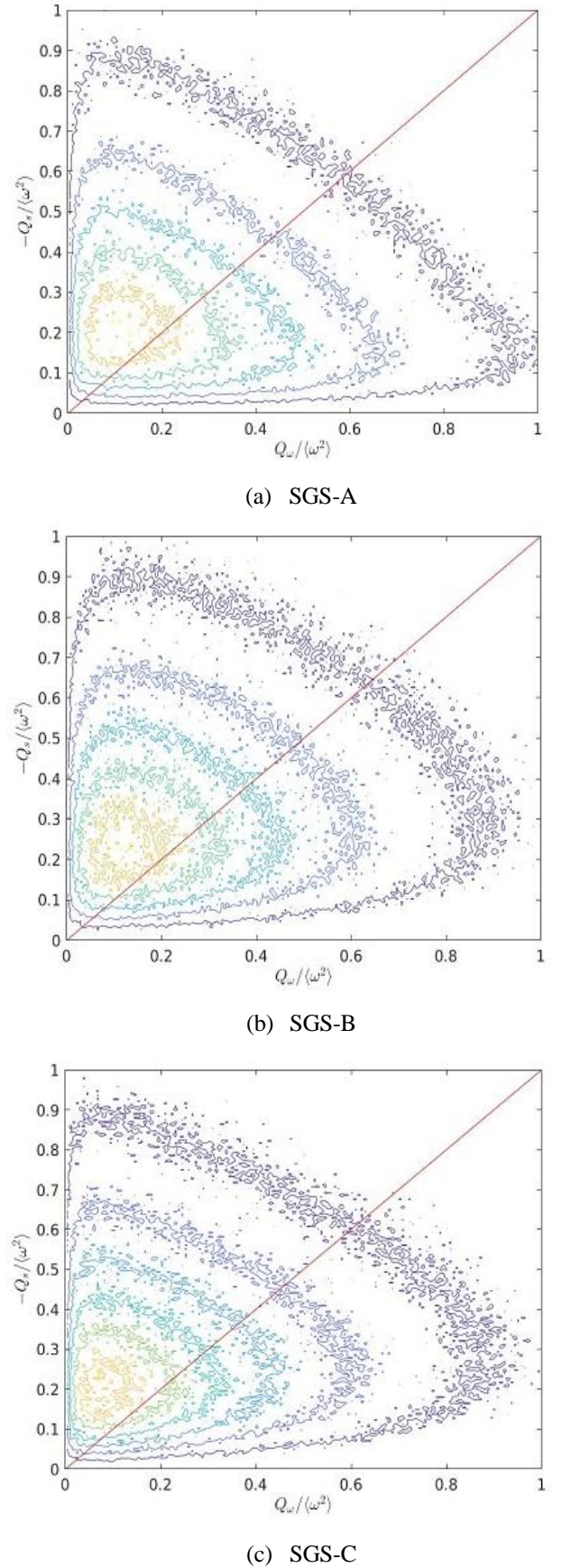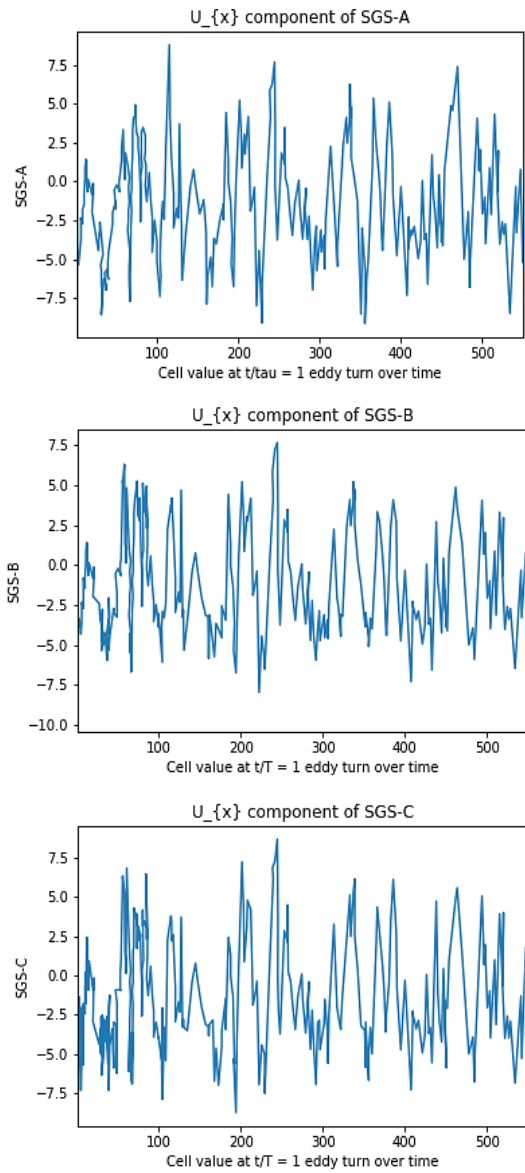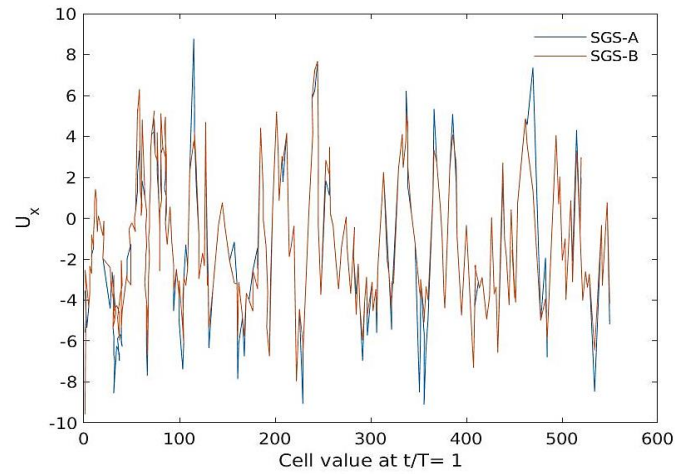

(a) SGS-A

(b) SGS-B

(c) SGS-C

Fig. 4 The JPDF between the second invariant of strain rate ($-Q_S$) and second invariant of rotation rate (Q_w)

Fig. 5 Cell value of U_x at $\frac{t}{T} = 1$ eddy turn-over time of the SGS models.

(a)   SGS-A v/s SGS-B

(b)   SGS-A v/s SGS-C

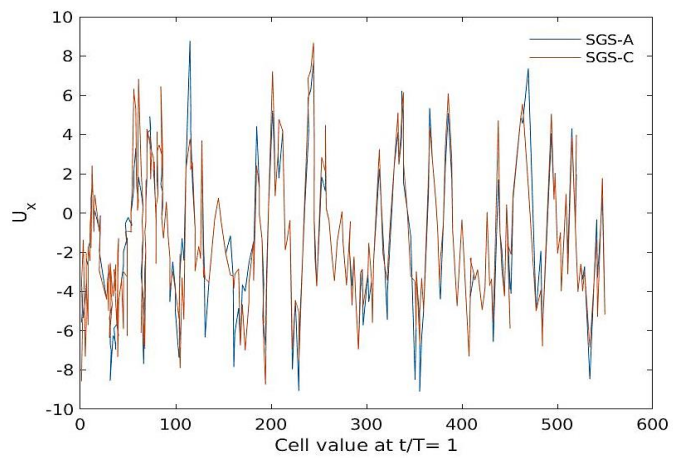Fig. 6 Comparing the shape of SGS-A with SGS-B and SGS-C subgrid models.

Before examining the correlation between the SGS models, this article shows some general statistics and covariance of U_x datasets of the SGS models. Since the covariance (COV) between SGS-A and SGS-B is 10.70 and between SGS-A and SGS-C is 11.03. These are the positive covariance; see Table 1. It indicates that the variables change in the same direction as we expect.

Now, Pearson's correlation (PC) and Spearson's correlation (SC) have been studied between the subgrid models. The PC and SC are useful to study to summarize the strength of a linear relationship between the datasets. Table 2 and Table 3, clearly state that the velocity component U_x of the SGS models have positive correlations. The Pearson's correlation of SGS-A between SGS-B and SGS-C are 0.9 and 0.8, whereas Spearson's correlation of SGS-A between SGS-B and SGS-C are 0.9 and 0.9, respectively.

Table 1 Comparing the statistical performance of SGS models for the U_x component.

Models	Mean	25%	50%	75%	STD	COV
SGS-A	-1.36	-3.82	-1.40	0.82	3.46	-
SGS-B	-1.18	-3.63	-1.82	0.86	3.27	-
SGS-C	-1.25	-3.69	-1.78	0.96	3.55	-
SGS-A v/s SGS-B	-	-	-	-	-	10.70
SGS-A v/s SGS-C	-	-	-	-	-	11.03

Table 2 Comparing the Pearson's correlation of the SGS models

SGS Models	Variable	Pearson's correlation
SGS-A v/s SGS-B	U_x	0.9
SGS-A v/s SGS-C	U_x	0.8

Table 3 Comparing Spearson's correlation of the SGS models

SGS Models	Variable	Spearson's correlation
SGS-A v/s SGS-B	U_x	0.9
SGS-A v/s SGS-C	U_x	0.9

The correlation matrices are plotted regarding three SGS models data in Fig. 7, see more details in [1],[19]. It is showing an excellent performance with Pearson's correlation and Spearman's correlation values. Moreover, all three SGS models are presented like Gaussian distribution in Fig. 7.
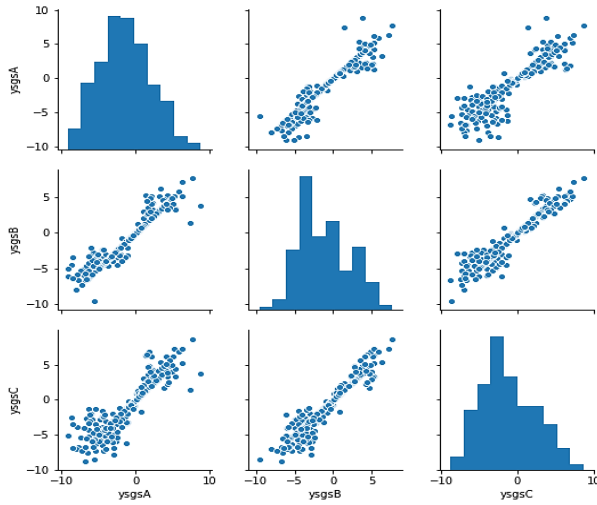

(a)
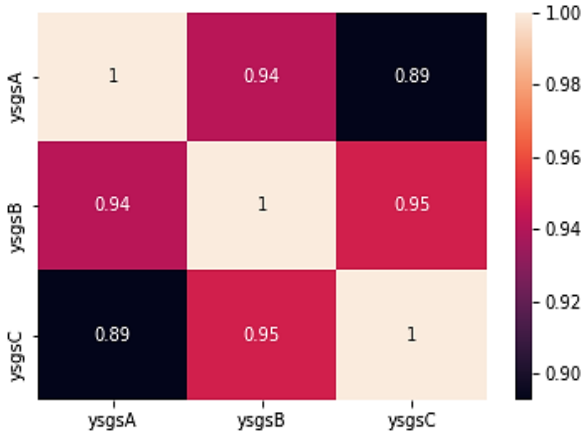
(b)

Fig. 7 (a) Pair plots, and (b) correlation matrix of U_x component between the SGS models

Finally, Gradient decent algorithm has been studied to identify the performance of SGS models. So, in order to train the machine learning and deep learning models, gradient decent is one of the most popular iterative optimization algorithms [20]. It is useful in finding the local minimum of a function. The main advantage of using a gradient decent algorithm is to minimize the cost function using iteration. However, the cost function is described as the measurement of the difference or inaccuracy between the current position's actual values and expected values, and it takes the form of a single real integer. In Fig. 8, gradient decent has been shown for the U_x component of SGS-A and SGS-B models.

Similarly, gradient decent has been shown for the U_x component of SGS-A and SGS-C models in Fig. 8. Corresponding linear regression plots of U_x component for SGS models present well performance by obtaining the minimum bias, see Fig. 8. Both figures are showing similar weights of 0.9, and a minimum cost between SGS-A and SGS-B is 1.22, whereas the minimum cost between SGS-A and SGS-C is 2.5.
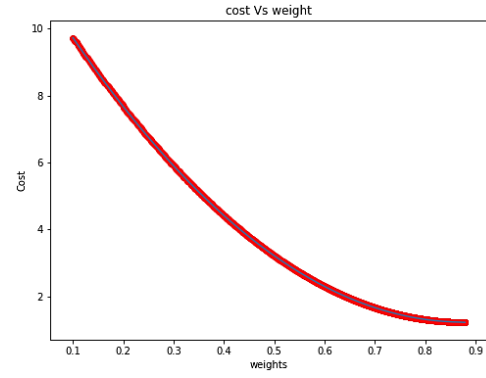
(a) Plot of cost v/s weight of U_x data between SGS-A and SGS B models.
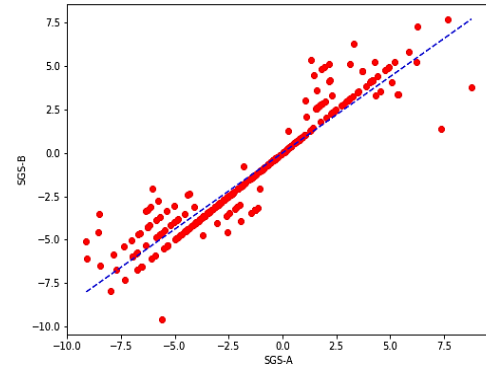
(b) Liner regression plot of U_x between SGS-A and SGS-B models.
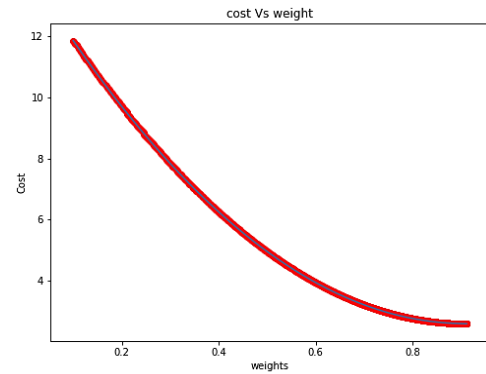
(c) Plot of cost v/s weight of U_x data between SGS-A and SGS-C models.

Fig. 8 Plot of cost v/s weight of U_x data between SGS models

6 Conclusion and Future Scope

The present article is focused on the subgrid-scale dissipation and production of turbulence generation, which is significantly influenced by the potential role of vortex stretching. The concept of this article learns through the statistical and machine learning approaches. For this purpose, the vortex stretching-based model SGS-A is used to demonstrate the SGS dissipation and validated with other two dynamic SGS models, such as SGS-B and SGS-C. The performance of the SGS-A model is well agreed with SGS-B and SGS-C models. Specifically, the loss of turbulence is more correlated to the turbulence production in the SGS-A model compared with the other SGS models. The JPDF of SGS model is presented the vortex stretching and sheetlike dissipation in the models and

indicates a playing role in a turbulent flow. Hence, this study suggests that the vortex stretching mechanism cascades energy.

These findings suggest that a turbulence model can effectively learn about the SGS dissipation from singular values of the velocity gradient tensor. The findings of JPDF of invariants of the velocity gradient tensor suggest that we may further learn about JPDF for higher resolution of LES data. Other possible further applications can include, such as magneto hydrodynamics, Ocean atmosphere, aerodynamics, fluid-solid interactions, etc.

References

[1] Smagorinsky, J., 1963. General circulation experiments with the primitive equations: I. The basic experiment. *Monthly Weather Review*, *91*(3), pp.99-164.

[2] Taylor, G.I., 1938. Production and dissipation of vorticity in a turbulent fluid. *Proceedings of the Royal Society of London. Series A-Mathematical and Physical Sciences*, *164*(916), pp.15-23.

[3] Carbone, M. and Bragg, A.D., 2020. Is vortex stretching the main cause of the turbulent energy cascade?. *Journal of Fluid Mechanics*, *883*.

[4] Sagaut, P. and Cambon, C., 2008. *Homogeneous turbulence dynamics* (Vol. 10). Cambridge: Cambridge University Press.

[5] Pope, S.B. and Pope, S.B., 2000. *Turbulent flows*. Cambridge university press.

[6] Nicoud, F. and Ducros, F., 1999. Subgrid-scale stress modelling based on the square of the velocity gradient tensor. *Flow, turbulence and Combustion*, *62*(3), pp.183-200..

[7] Davidson, P. (2004). Turbulence: an introduction for scientists and engineers. Oxford University Press.

[8] Hossen, M.K., Mulayath Variyath, A. and Alam, J.M., 2021. Statistical Analysis of Dynamic Subgrid Modeling Approaches in Large Eddy Simulation. *Aerospace*, *8*(12), p.375.

[9] Kim, W.W. and Menon, S., 1995. A new dynamic one-equation subgrid-scale model for large eddy simulations. In *33rd Aerospace Sciences Meeting and Exhibit* (p. 356).

[10] Meneveau, C., 2010. Turbulence: Subgrid-scale modeling. *Scholarpedia*, *5*(1), p.9489.

[11] Deardorff, J.W., 1972. Numerical investigation of neutral and unseq planetary boundary layers. *Journal of Atmospheric Sciences*, *29*(1), pp.91-115.

[12] Hossen, M. K., Variyath, A., & Alam, J., 2021. Statistical analysis of the role of vortex stretching in large eddy simulation. *Proceedings of the 29th Annual Conference of the Computational Fluid Dynamics Society of Canada. CFDSC2021*. July 27-29, Online.

[13] Martın, J., Ooi, A., Chong, M.S. and Soria, J., 1998. Dynamics of the velocity gradient tensor invariants in isotropic turbulence. *Physics of Fluids*, *10*(9), pp.2336-2346.

[14] Jeong, J. and Hussain, F., 1995. On the identification of a vortex. *Journal of Fluid Mechanics*, *285*, pp.69-94.

[15] Perry, A.E. and Chong, M.S., 1994. Topology of flow patterns in vortex motions and turbulence. *Applied Scientific Research*, *53*(3), pp.357-374.

[16] Martın, J., Ooi, A., Chong, M.S. and Soria, J., 1998. Dynamics of the velocity gradient tensor invariants in isotropic turbulence. *Physics of Fluids*, *10*(9), pp.2336-2346.

[17] Dallas, V. and Alexakis, A., 2013. Structures and dynamics of small scales in decaying magnetohydrodynamic turbulence. *Physics of Fluids*, *25*(10), p.105106.

[18] da Silva, C.B. and Pereira, J.C., 2008. Invariants of the velocity-gradient, rate-of-strain, and rate-of-rotation tensors across the turbulent/nonturbulent interface in jets. *Physics of Fluids*, *20*(5), p.055101.

[19] Hossen, M.K., 2022. Heart Disease Prediction Using Machine Learning Techniques. *American Journal of Computer Science and Technology*, *5*(3), pp.146-154.

[20] Wikipedia contributors. (2022, June 28). Gradient descent. In Wikipedia, The Free Encyclopedia. Retrieved 05:31, July 23, 2022, from https://en.wikipedia.org/w/index.php?title=Gradient_descent&oldid=1095507248.